Bio-Integrated Autonomous Infrastructure: A Coherence-Based Architecture for Living Scaffolds in Structural and Ecological Monitoring

Allison Hensgen* Iulia Koplik† Joel Thorarinson‡

June 2026

Abstract

Living biological systems — mycelium networks, microbial biofilms, biomineralized scaffolds — sense, adapt, self-repair, and harvest energy from their environment without manufactured components. These are engineering capabilities, not metaphors. We propose a six-layer platform architecture that integrates living biological scaffolds into autonomous infrastructure monitoring: (1) a *biological scaffold network* providing the physical substrate, (2) a *sensing layer* making biological dynamics electrically observable, (3) an *energy harvesting layer* powering the system from biological and environmental sources, (4) a *signal processing layer* converting raw signals into state variables, (5) an *AI orchestration layer* — the Coherence Engine — that monitors system health using the composite operator $\Delta = (P \cdot A \cdot R)/(D + N)$ validated across seven physical domains [Thorarinson and Hensgen, 2026], and (6) an *application interface* exposing system state to operators. We develop two applications in detail: structural health monitoring with mycelium-augmented bio-concrete, where the coherence engine tracks both structural integrity and biological healing capacity; and ecological monitoring with soil-embedded mycelium networks, where distributed biological sensing detects environmental transitions at lower cost and higher spatial density than conventional sensor arrays. We specify four operational modes with quantitative transition criteria, present a concrete prototype design (estimated materials cost: $180–$350), and discuss coherence threshold calibration for biological substrates.

Keywords: bio-integrated infrastructure; mycelium networks; microbial fuel cells; coherence engine; structural health monitoring; ecological monitoring; living materials; bioelectric signaling; AI orchestration

1 Introduction

Modern infrastructure monitoring treats buildings, bridges, and ecosystems as objects to be observed by external sensors manufactured from silicon, powered by batteries, and maintained by human operators. This approach works, but it carries intrinsic limitations: sensor networks degrade, batteries require replacement, and spatial coverage is constrained by the cost of individual sensor nodes. Meanwhile, the biological systems that colonize, inhabit, and interact with infrastructure — fungal mycelium in soil and concrete, microbial biofilms on surfaces, biomineralized deposits — are already sensing, transducing, and responding to the same environmental variables that engineered sensors measure. They do so continuously, at high spatial density, with self-repair capability, and at near-zero energy cost.

This is not a new observation. Proposals for "living architecture" — buildings that grow, metabolize, and adapt — have been articulated for over a decade [Armstrong, 2012], and ecological

*Coherence Research Group. ORCID: 0009-0008-7247-0307
†Coherence Research Group. ORCID: 0009-0005-3765-4811
‡Coherence Research Group. ORCID: 0000-0002-0553-842X. joel.thorarinson@conformalmaps.com

engineering has long recognized that designed ecosystems can perform infrastructure functions [Mitsch and Jørgensen, 2004]. What has been missing is an integration architecture: a formal framework that connects biological dynamics to engineering decision-making through a defined stack of sensing, processing, and AI orchestration layers.

The biological materials are ready. Mycelium composites achieve compressive strengths of 0.17–0.55 MPa with Young's moduli of 5–50 MPa depending on species and substrate [Haneef et al., 2017], and thermal conductivities of 0.04–0.08 W/m·K suitable for building insulation [Elsacker et al., 2019]. Bio-concrete incorporating *Bacillus* spores self-heals cracks up to 0.8 mm through metabolically driven calcium carbonate precipitation [Jonkers et al., 2010]. Living building materials produced from *Synechococcus* cyanobacteria in sand-gelatin matrices achieve compressive strengths of 1–4 MPa and can regenerate, with a single parent brick producing up to eight offspring over three generations [Heveran et al., 2020]. Microbial fuel cells generate current densities of 0.1–10 A/m^2 from organic substrates [Logan et al., 2006, Logan, 2009]. Engineered biofilms with programmable curli nanofibers provide tunable adhesion, catalytic, and templating properties [Nguyen et al., 2014]. Synthetic biology enables design of living functional materials with specified mechanical, optical, and chemical properties at the genetic level [Tang et al., 2021].

The AI layer is also ready. The Coherence Engine [Thorarinson and Hensgen, 2026] — validated on turbofan engines, cardiac rhythms, industrial valves, power grids, EEG signals, financial time series, and synthetic benchmarks — measures whether a complex system is maintaining its structural organization or losing coherence, using a composite operator $\Delta = (P \cdot A \cdot R)/(D + N)$ that is agnostic to the physical substrate producing the time series. A mycelium network under drought stress and a turbofan engine losing bearing integrity produce the same mathematical signature: declining pattern retention, desynchronization across channels, and reduced recovery capacity after perturbation.

This paper connects these two bodies of work. We define a six-layer architecture for bio-integrated infrastructure monitoring, develop two applications in full technical detail — structural health monitoring and ecological monitoring — and specify a prototype that is buildable with existing components.

1.1 Contributions

1. A **six-layer architecture** for bio-integrated autonomous infrastructure, with formal interface specifications and failure modes for each layer.
2. Technical demonstration that the **Coherence Engine** provides a natural AI orchestration layer for living systems, with explicit discussion of threshold calibration for biological substrates.
3. Two **detailed application designs**: mycelium-augmented structural health monitoring and mycelium-based ecological monitoring, with sensor configurations, energy budgets, and expected performance characteristics.
4. **Four operational modes** with quantitative transition criteria (Δ thresholds, energy budget ratios, baseline duration requirements).
5. A **concrete prototype specification** with bill of materials, estimated cost ($180–$350), and 17-day experimental protocol.

2 Background: Biological Scaffolds as Engineering Materials

2.1 Mycelium Networks

Fungal mycelium forms dense, branching networks through substrates (soil, wood, agricultural waste) with electrically active hyphae that exhibit spontaneous spiking behavior at 0.03–0.3 Hz

[Adamatzky, 2018a]. The spiking patterns respond to mechanical pressure, chemical gradients, temperature, and moisture with measurable changes in frequency, amplitude, and inter-spike intervals. Adamatzky has further demonstrated that mycelium geometry can implement computation, with information represented by electrical spikes and logic gates realized through network topology [Adamatzky, 2018b].

As a structural material, mycelium composites have been characterized systematically. Haneef et al. [2017] showed that *Ganoderma lucidum* and *Pleurotus ostreatus* produce composites with Young's moduli of 5–50 MPa, tunable by species selection and growth conditions. Elsacker et al. [2019] demonstrated that fiber size exerts greater influence on mechanical strength than fiber type across lignocellulosic substrates, and confirmed thermal conductivities (0.04–0.08 W/m·K) meeting building insulation requirements. These are measured material properties, not projections.

2.2 Microbial Biofilms and Bio-Concrete

Bacterial and archaeal communities form structured biofilms on surfaces, generating measurable electrical potential through extracellular electron transfer. *Geobacter* and *Shewanella* species produce current densities of 0.1–10 A/m^2 from organic substrates [Logan et al., 2006, Logan, 2009]. Biofilm impedance, current output, and metabolic activity vary with nutrient availability, temperature, pH, and toxin exposure, providing multiple observable channels. Nguyen et al. [2014] demonstrated genetically encoded curli nanofiber display systems that confer specified adhesion, catalytic, and templating properties to *E. coli* biofilm matrices, establishing that biofilm functionality can be engineered at the genetic level.

Self-healing bio-concrete represents the most mature application of living materials in infrastructure. Jonkers et al. [2010] demonstrated that alkali-resistant *Bacillus* spores embedded with calcium lactate nutrients in concrete self-heal cracks up to 0.8 mm through metabolically driven calcium carbonate precipitation. Heveran et al. [2020] extended this to create living building materials from *Synechococcus* cyanobacteria in sand-gelatin matrices, achieving 15% greater fracture toughness than abiotic controls, compressive strengths of 1–4 MPa, and regenerative capacity across three generations. Whole-cell biosensors embedded in biological scaffolds can detect specific analytes (heavy metals, organic pollutants, quorum-sensing molecules) at sub-micromolar concentrations [van der Meer and Belkin, 2010].

2.3 Biological Communication and Coordination

Living scaffolds are not passive substrates awaiting external instrumentation. They implement distributed sensing and collective decision-making through endogenous signaling networks.

Levin [2021] demonstrated that endogenous voltage gradients produced by ion channels and gap junctions serve as reprogrammable circuits encoding spatial information for embryogenesis, regeneration, and cancer suppression. These bioelectric patterns constitute a layer of information processing between the molecular (genetic) and organismal scales [Levin, 2023]. Levin's framework of "collective intelligence" across biological scales [McMillen and Levin, 2024] provides a theoretical basis for understanding how scaffold-level coherence emerges from the coordinated electrical activity of constituent cells — a mechanism directly relevant to the coherence monitoring we propose.

Additional biological communication channels have been identified at the subcellular level. Kumar et al. [2016] demonstrated through FDTD modeling that myelinated axons can function as photonic waveguides, with the myelin sheath's refractive index (1.44) relative to the axon interior (1.38) and interstitial fluid (1.34) supporting guided optical modes. Zangari et al. [2018] modeled nodes of Ranvier as nanoantenna arrays generating electromagnetic radiation in the 300–2500 nm range. Patwa et al. [2024] demonstrated superradiant enhancement in tryptophan networks within microtubules, actin filaments, and amyloid fibrils, with quantum yield robust against thermal noise. These findings establish that biological scaffolds contain endogenous optical communication

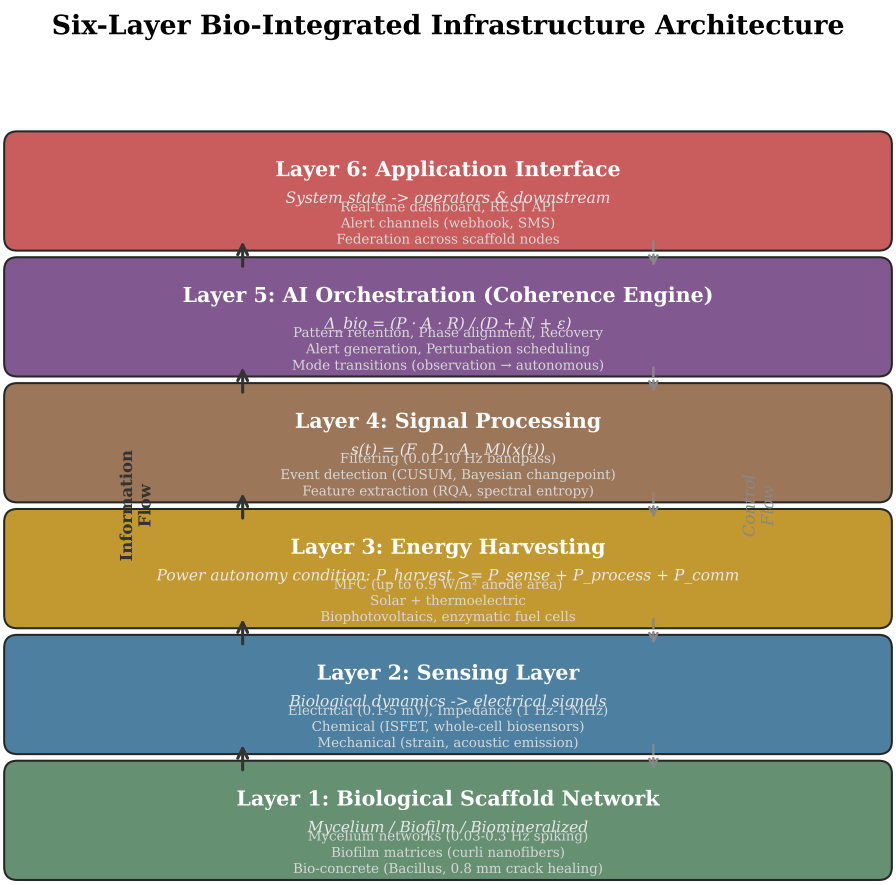

Figure 1: Six-layer bio-integrated infrastructure architecture. Information flows upward from the biological scaffold through sensing, energy harvesting, signal processing, and AI orchestration to the application interface. Control flows downward. Each layer has a defined interface to adjacent layers, enabling modular substitution of scaffold types, sensing modalities, and processing hardware.

channels, though the engineering implications for macroscale infrastructure integration remain to be characterized.

3 The Six-Layer Architecture

The platform consists of six layers, each with a defined interface to adjacent layers (Figure 1). Information flows upward (biological dynamics → electrical signals → processed state → AI assessment → application output) and control flows downward (application commands → AI decisions → perturbation signals → environmental modifications → biological response).

3.1 Layer 1: Biological Scaffold Network

Definition 1 (Biological Scaffold)**.** *A biological scaffold $\mathcal{B}$ is a living or bio-derived material system that:*

1. *occupies a spatial domain $\Omega \subset \mathbb{R}^3$ with time-varying boundary $\partial\Omega(t)$,*

2. *exhibits measurable electrical, chemical, or mechanical dynamics,*

3. *responds to environmental perturbations on timescales* $\tau_{response} \in [10^0, 10^6]$ *seconds,*

4. *is capable of growth, adaptation, or self-repair.*

For the two applications developed in this paper, two scaffold classes are relevant:

Mycelium networks serve as the primary scaffold for both applications. In ecological monitoring, *Pleurotus ostreatus* mycelium colonizes soil substrates, forming networks that sense chemical gradients, moisture, temperature, and mechanical stress through changes in electrical spiking patterns (0.03–0.3 Hz, amplitude 0.1–5 mV). In structural health monitoring, mycelium composites are integrated into concrete panels alongside bacterial healing agents. In both cases, the scaffold's bioelectric activity — which Levin's work identifies as the medium of collective biological intelligence [McMillen and Levin, 2024] — provides a continuous readout of system state.

Biomineralized and hybrid scaffolds are relevant to the structural health monitoring application. Bio-concrete incorporating *Bacillus* spores with calcium lactate nutrients [Jonkers et al., 2010] provides both mechanical function and self-healing capacity. The coherence engine monitors the viability of the bacterial population through impedance and metabolic channels, detecting loss of healing capacity before cracks exceed the self-repair threshold. Hybrid scaffolds combining living biofilms with engineered substrates (3D-printed lattices, electrospun fibers) extend this approach to materials with both biological responsiveness and mechanical performance.

3.2 Layer 2: Sensing Layer

Definition 2 (Sensing Layer)**.** *The sensing layer* $\mathcal{S}$ *is a set of transducers* $\{s_1, \ldots, s_n\}$ *that convert biological dynamics in* $\mathcal{B}$ *to electrical signals* $\mathbf{x}(t) \in \mathbb{R}^n$*, where each* s_i *has:*

- *a measurement modality (electrical, impedance, chemical, thermal, mechanical),*
- *a sampling rate* $f_i \geq 2f_{Nyquist}$ *for the biological process of interest,*
- *a noise floor* σ_i *below the signal amplitude of the biological dynamics.*

Five sensing modalities are relevant to bio-integrated scaffolds:

Electrical potential. Differential voltage measurements between electrodes inserted into or placed on the scaffold surface. Mycelium spiking activity produces signals of 0.1–5 mV below 1 Hz. Biofilm redox potential indicates metabolic state. Requirements: high-impedance amplifiers (>10 MΩ), 16-bit minimum ADC resolution.

Electrochemical impedance. Swept-frequency impedance spectroscopy (1 Hz–1 MHz) characterizes the scaffold's electrical properties as a function of frequency. Changes in impedance spectra indicate structural reorganization, moisture variation, biomass density changes, or cell viability shifts. Four-electrode configurations provide spatially resolved measurements.

Chemical sensing. pH, dissolved oxygen, CO_2, volatile organic compounds (VOCs), and specific ion concentrations. ISFET arrays provide multi-analyte sensing at the scaffold interface. In bio-integrated systems, whole-cell biosensors offer an alternative: engineered reporter bacteria detect specific analytes at sub-micromolar concentrations with high specificity [van der Meer and Belkin, 2010], turning the scaffold itself into a distributed chemical sensor.

Environmental parameters. Temperature (thermocouples, thermistors), relative humidity (capacitive sensors), light intensity (photodiodes), and barometric pressure. These provide context for interpreting biological signals — a change in mycelium spiking frequency may reflect a temperature change rather than scaffold stress.

Mechanical sensing. Strain gauges, piezoelectric sensors, and MEMS accelerometers detect deformation, vibration, and acoustic emissions. For structural health monitoring, these conventional channels are combined with biological channels (impedance changes in self-healing bacteria, bioelectric signals from embedded organisms), extending the SHM paradigm of Farrar and Worden [2007] with biological sensing modalities.

3.3 Layer 3: Energy Harvesting

Definition 3 (Energy Harvesting Layer)**.** *The energy harvesting layer $\mathcal{E}$ provides power $P_{harvest}(t)$ to the sensing and processing layers, where the system is operationally autonomous when:*

$$\bar{P}_{harvest} \geq P_{sense} + P_{process} + P_{comm} \tag{1}$$

averaged over the duty cycle period, with P_{sense}, $P_{process}$, and P_{comm} the power requirements for sensing, signal processing, and communication respectively.

Three energy harvesting pathways are relevant:

Microbial fuel cells (MFCs). Electrochemically active microorganisms oxidize organic substrates and transfer electrons to an anode [Logan et al., 2006, Logan, 2008]. Exoelectrogenic bacteria achieve anode power densities up to 6.9 $\mathrm{W/m^2}$ under optimized conditions, with Coulombic efficiencies reaching 90% [Logan, 2009]. MFC output is continuous but low-power (typically 0.1–1 mW for small-scale systems), suitable for intermittent sensing with duty cycling.

Environmental harvesting. Thin-film solar cells provide 10–100 $\mathrm{mW/cm^2}$ under direct illumination. Thermoelectric generators exploiting temperature differentials between scaffold interior and ambient air produce 1–50 $\mu\mathrm{W/cm^2}$. For the ecological monitoring application, a 5 W solar panel with lithium-polymer battery provides 24-hour operation.

Hybrid strategy. Near-term prototypes use external power (USB, battery, grid) supplemented by MFC and solar sources. The energy budget is characterized during the observation mode to determine whether full energy autonomy is achievable for a given deployment.

3.4 Layer 4: Signal Processing

Definition 4 (Signal Processing Layer)**.** *The signal processing layer $\mathcal{P}$ transforms raw sensor signals $\mathbf{x}(t) \in \mathbb{R}^n$ into a state vector $\mathbf{s}(t) \in \mathbb{R}^m$ where $m \leq n$, through a pipeline:*

$$\mathbf{s}(t) = \mathcal{P}(\mathbf{x}(t)) = (\mathcal{F} \circ \mathcal{D} \circ \mathcal{A} \circ \mathcal{M})(\mathbf{x}(t)) \tag{2}$$

where $\mathcal{M}$ maps raw signals to standardized units, $\mathcal{A}$ detects anomalous events, $\mathcal{D}$ performs dimensionality reduction, and $\mathcal{F}$ extracts features relevant to the coherence assessment.

The processing pipeline comprises four stages:

Filtering and conditioning ($\mathcal{M}$). Bandpass filtering to isolate biological signal bands (0.01–1 Hz for mycelium spiking, 1 Hz–1 MHz for impedance spectroscopy), notch filtering for power line interference rejection, baseline drift removal via high-pass filtering or polynomial detrending, and unit conversion to physical quantities.

Event detection ($\mathcal{A}$). Spike detection in electrical signals using threshold crossing with dead-time enforcement. Anomaly detection via adaptive thresholds (median absolute deviation, exponentially weighted moving average). State change detection via CUSUM or Bayesian changepoint methods [Adams and MacKay, 2007]. Events are timestamped and classified (spike, burst, transition, artifact).

Dimensionality reduction ($\mathcal{D}$). Principal component analysis or independent component analysis to extract dominant modes of variation from multi-channel sensor data, reducing input dimensionality to the AI layer while preserving variance structure.

Feature extraction ($\mathcal{F}$). Computation of time-domain features (spike rate, inter-spike interval statistics, signal variance, kurtosis), frequency-domain features (power spectral density, spectral entropy, peak frequency), and recurrence features (recurrence rate, determinism, laminarity, entropy of diagonal line lengths) serving as inputs to the coherence operator.

3.5 Layer 5: AI Orchestration — The Coherence Engine

Definition 5 (Bio-Coherence Score)**.** *For the processed state vector* $\mathbf{s}(t) \in \mathbb{R}^m$ *from the biological scaffold system, the bio-coherence score is:*

$$\Delta_{bio}(t) = \frac{P(t) \cdot A(t) \cdot R(t)}{D(t) + N(t) + \epsilon} \tag{3}$$

where the five operators are computed on the biological state time series as defined for engineered systems in Thorarinson and Hensgen [2026]:

- $P(t)$*:* ***Pattern retention*** *— does the scaffold maintain recurring dynamical patterns (spike rhythms, impedance cycles, metabolic oscillations)?*
- $A(t)$*:* ***Phase alignment*** *— are different regions/channels of the scaffold synchronized?*
- $R(t)$*:* ***Recovery capacity*** *— does the scaffold return to baseline after perturbation?*
- $D(t)$*:* ***Drift*** *— is the scaffold's statistical baseline shifting?*
- $N(t)$*:* ***Noise amplification*** *— is the scaffold amplifying stochastic perturbations?*

The coherence operator does not need to know it is measuring a biological system. A mycelium network losing moisture exhibits the same mathematical signatures as a turbofan engine losing bearing integrity: pattern retention P declines as regular spiking becomes irregular, phase alignment A drops as different network regions desynchronize, and recovery capacity R decreases as the system fails to return to baseline after perturbation.

The extended operators refine the assessment for specific biological degradation modes. Memory-of-Attractor (M) detects whether the scaffold has lost its normal dynamical attractor (e.g., a biofilm that has lost its circadian metabolic rhythm). Windowed Recovery (W) measures recovery from controlled perturbations (e.g., how quickly mycelium spiking returns to baseline after a temperature pulse). Loss-of-Flower (L) detects loss of quasi-stationary states (e.g., a biomineralized scaffold no longer settling into stable mechanical equilibria after loading).

3.5.1 Coherence Threshold Calibration for Biological Systems

The threshold values $\Delta > 0.7$ (healthy), $0.3 < \Delta < 0.7$ (transition), and $\Delta < 0.3$ (degraded) were established on engineering datasets (turbofan engines, industrial valves) in Thorarinson and Hensgen [2026]. Biological systems require domain-specific recalibration for three reasons:

Higher baseline variability. Living systems exhibit greater stochastic variation than engineered systems. A healthy mycelium network may have a baseline Δ of 0.5–0.8 rather than the 0.8–1.0 typical of a healthy turbofan engine, because biological spike patterns are inherently more variable than combustion cycles. Calibration requires establishing the per-instance baseline distribution of Δ during a dedicated observation period (minimum 72 hours for mycelium, 48 hours for biofilms) before setting alert thresholds.

Slower timescales. Biological degradation unfolds over hours to weeks, not minutes. The window size for computing Δ must be adjusted: 5–15 minute windows (vs. 30-second windows for engines) for mycelium spiking dynamics, with multi-scale analysis at 1-hour and 24-hour windows to capture diurnal and seasonal patterns.

Environmental coupling. Temperature, humidity, and nutrient availability directly modulate biological dynamics. A temperature drop from 25°C to 15°C will reduce mycelium spiking frequency without indicating degradation. The calibration procedure must establish Δ as a function of environmental covariates, using the environmental sensor channels (Layer 2) to distinguish environmentally driven coherence changes from pathological degradation. We propose a conditional threshold: $\Delta_{\text{alert}}(T, H) = \Delta_{\text{baseline}}(T, H) - k \cdot \sigma_{\Delta}(T, H)$, where the baseline and

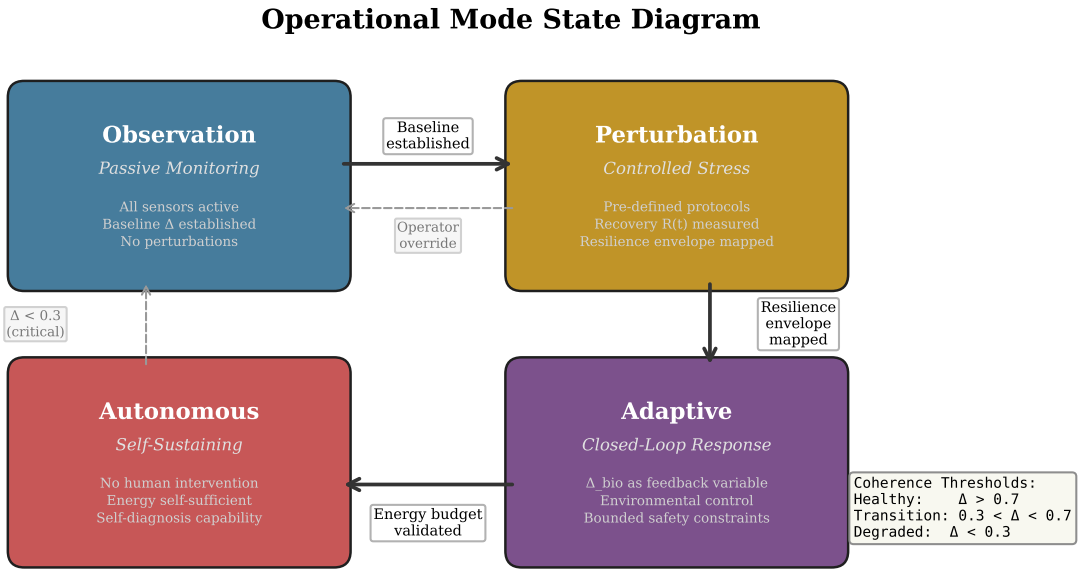

Figure 2: Operational mode state diagram. Solid arrows indicate forward transitions as system capabilities are validated; dashed arrows indicate fallback transitions triggered by coherence degradation or operator override. Each transition has defined quantitative preconditions.

standard deviation are computed for binned temperature T and humidity H values, and k sets the alert sensitivity (we recommend $k = 2$ for the initial deployment, tightened to $k = 3$ after baseline characterization).

3.6 Layer 6: Application Interface

The application interface exposes the system's state and capabilities to operators and downstream systems through:

- **Real-time dashboard**: coherence score $\Delta_{\text{bio}}(t)$, individual operator values, sensor time series, alert history.
- **REST API**: programmatic access to current state, historical data, and control commands.
- **Alert channels**: push notifications via webhook, email, or SMS when coherence thresholds are crossed.
- **Data export**: time-series data and coherence assessments in standard formats for offline analysis.
- **Federation**: for networks of bio-integrated systems, aggregated coherence views across multiple scaffold nodes.

4 Operational Modes

The platform operates in four modes, representing increasing levels of autonomy (Figure 2). Each mode transition has quantitative preconditions.

4.1 Mode 1: Observation (Passive Monitoring)

All sensors active, continuous data acquisition, coherence computed in real time. No perturbations applied. The system records baseline dynamics and establishes the scaffold's normal operating envelope.

Coherence role: Establish baseline Δ_{bio} distribution, detect natural coherence transitions (seasonal changes in mycelium activity), generate alerts when coherence drops below historical norms.

Transition to Mode 2: Requires minimum 72 hours of baseline data with coefficient of variation $\text{CV}(\Delta_{\text{bio}}) < 0.3$, confirming that the baseline is stable enough for perturbation-response analysis.

4.2 Mode 2: Perturbation (Controlled Stress Testing)

The system applies controlled perturbations — temperature pulses, moisture changes, mechanical loads, chemical gradients — and measures the scaffold's response. Perturbation protocols are pre-defined and operator-approved.

Coherence role: Compute recovery capacity $R(t)$ and Windowed Recovery $W(t)$ from perturbation-response pairs. Map the scaffold's resilience envelope: the set of perturbation magnitudes from which the system recovers with $\Delta_{\text{bio}} > \Delta_{\text{baseline}} - 2\sigma$ within a defined recovery window.

Transition to Mode 3: Requires complete resilience envelope mapping for at least two perturbation types, with recovery time predictable to $\pm 20\%$.

4.3 Mode 3: Adaptive (Closed-Loop Response)

The coherence engine monitors Δ_{bio} in real time and triggers environmental adjustments when coherence degrades. If drought stress reduces mycelium coherence, the system increases moisture. If temperature fluctuation desynchronizes biofilm activity, the system activates thermal regulation. Control actions are bounded by safety constraints defined at deployment.

Coherence role: Closed-loop control where the coherence score is the primary feedback variable. The control objective is $\Delta_{\text{bio}}(t) > \Delta_{\text{target}}$, with the controller adjusting environmental parameters to maintain coherence above threshold.

Transition to Mode 4: Requires $\bar{P}_{\text{harvest}} \geq 1.2 \times (P_{\text{sense}} + P_{\text{process}} + P_{\text{comm}})$ sustained over 7 days (20% energy margin), and demonstrated closed-loop coherence maintenance over 30 days with $\Delta_{\text{bio}} > \Delta_{\text{target}}$ for $>95\%$ of the observation period.

4.4 Mode 4: Autonomous (Self-Sustaining Operation)

The system operates without human intervention for extended periods. Energy harvesting meets power requirements. The coherence engine manages scaffold health through adaptive environmental control.

Coherence role: Autonomous decision-making about perturbation scheduling, environmental control, power management (duty cycling sensors when coherence is stable, increasing sampling rate when coherence degrades), and self-diagnosis (distinguishing scaffold degradation from sensor failure based on coherence patterns across multiple channels).

Fallback: Any mode transitions to Mode 1 (observation) if $\Delta_{\text{bio}} < 0.1$ for more than 1 hour, if energy reserves drop below 10% of capacity, or upon operator override.

5 Application 1: Structural Health Monitoring with Mycelium-Augmented Bio-Concrete

5.1 Motivation

Structural health monitoring (SHM) is fundamentally a statistical pattern recognition problem [Farrar and Worden, 2007]: sensors measure structural response, signal processing extracts features, and algorithms classify the structural state. Bio-concrete incorporating self-healing bacterial spores adds a biological dimension: the structure can repair itself, but only if the bacterial population remains viable. Current SHM systems cannot monitor healing agent viability. We propose combining conventional SHM sensors with biological sensing channels, orchestrated by the coherence engine, to monitor both structural integrity and self-repair capacity.

5.2 System Configuration

Scaffold (Layer 1). Reinforced concrete panel ($1 \times 1 \times 0.15$ m) incorporating two biological systems: (a) *Bacillus* spores with calcium lactate nutrients for crack self-healing [Jonkers et al., 2010], and (b) mycelium composite inserts (four $5 \times 5 \times 5$ cm blocks of *Pleurotus ostreatus* on wood-chip substrate) embedded at the concrete surface to provide biological sensing channels.

Sensing (Layer 2). Twelve channels total:

- 4 strain gauges (foil type, 350 Ω) at panel quarter-points, measuring structural deformation at 100 Hz.
- 4 differential electrode pairs in mycelium inserts, measuring spiking activity at 250 Hz via 24-bit ADC (ADS1299).
- 2 impedance probes in the bio-concrete matrix, measuring bacterial viability via swept-frequency impedance spectroscopy (1 Hz–100 kHz, sweep every 5 minutes).
- 1 temperature sensor (SHT31), 1 humidity sensor (capacitive), providing environmental context.

Energy (Layer 3). Grid power for permanent structural installations. For remote bridge or overpass monitoring, a 10 W solar panel with 20 Wh lithium-polymer battery and optional soil-based MFC at the foundation.

Processing (Layer 4). Raspberry Pi 4 (4 GB) or equivalent edge compute. Bandpass filtering on mycelium channels (0.01–10 Hz), strain gauge conditioning, and impedance spectrum processing. Feature extraction: spike rate, inter-spike interval statistics, spectral entropy, recurrence quantification metrics computed in 5-minute sliding windows with 1-minute step. Strain features: peak strain, strain rate, frequency content.

AI Orchestration (Layer 5). Coherence engine computing Δ_{bio} on the combined biological channels (mycelium spiking + bacterial impedance) and Δ_{struct} on the structural channels (strain gauges). A composite health score $H = w_1\Delta_{\text{struct}} + w_2\Delta_{\text{bio}}$ with $w_1 = 0.6$, $w_2 = 0.4$ (structural integrity weighted higher than healing capacity) provides the primary monitoring output.

5.3 Expected Performance

The system provides two capabilities beyond conventional SHM:

Healing capacity monitoring. When Δ_{bio} declines while Δ_{struct} remains stable, the biological healing agents are losing viability even though the structure is currently intact. This provides advance warning that the self-repair capacity is degrading — a condition invisible to conventional strain-only SHM systems.

Biological early warning. Mycelium inserts at the concrete surface respond to moisture ingress, chemical changes (carbonation, chloride penetration), and micro-cracking through changes in spiking patterns before these processes produce measurable strain. The biological channels may detect degradation precursors that mechanical sensors miss.

Alert thresholds for the structural application: watch ($H < 0.65$), warning ($H < 0.45$), critical ($H < 0.25$), with separate alerts for biological-only degradation ($\Delta_{\text{bio}} < 0.3$ while $\Delta_{\text{struct}} > 0.7$).

6 Application 2: Ecological Monitoring with Soil-Embedded Mycelium Networks

6.1 Motivation

Conventional ecological monitoring networks deploy discrete sensor nodes at spacings of meters to kilometers, creating spatial gaps where environmental transitions go undetected. A mycelium network colonizing soil provides a continuous biological sensor over areas of square meters to hectares, with each hyphal tip acting as a chemical and mechanical transducer. Manufacturing an equivalent sensor network at this spatial density would cost orders of magnitude more and lack self-repair capability.

6.2 System Configuration

Scaffold (Layer 1). *Pleurotus ostreatus* mycelium colonizing a wood-chip substrate in a $30 \times 30 \times 10$ cm container, placed in soil at the monitoring site. Full colonization occurs in 2–4 weeks. For network deployment, multiple containers at 2–5 m spacing create a distributed monitoring array.

Sensing (Layer 2). Six channels per node:

- 4 differential electrode pairs (stainless steel, 1 mm diameter, 50 mm spacing) inserted into the substrate at cardinal positions, sampling at 250 Hz via 24-bit ADC.
- 1 temperature/humidity sensor (SHT31).
- 1 soil moisture sensor (capacitive).

Energy (Layer 3). 5 W solar panel with 10 Wh lithium-polymer battery for 24-hour operation. Soil-based MFC supplements solar with 0.1–1 mW continuous output. Power budget: sensing 50 mW (duty-cycled), processing 500 mW (Raspberry Pi, duty-cycled), communication 100 mW (periodic), yielding average consumption of approximately 200 mW with 10% duty cycling on processing.

Processing (Layer 4). Raspberry Pi 4 (4 GB). Bandpass filter (0.01–10 Hz) on electrical channels. Spike detection via adaptive threshold (3σ above median). Feature extraction: spike rate, inter-spike interval coefficient of variation, spectral entropy, and RQA metrics (recurrence rate, determinism) computed in 300-second sliding windows with 60-second step.

AI Orchestration (Layer 5). Coherence engine computing Δ_{bio} every 60 seconds. Conditional alert thresholds $\Delta_{\text{alert}}(T, H)$ as described in Section 3.5.1, accounting for temperature and humidity effects on baseline spiking dynamics. For multi-node deployments, spatial coherence (cross-correlation of Δ across nodes) detects spatially propagating environmental transitions (advancing drought front, contamination plume).

6.3 Expected Performance

The system detects environmental transitions as changes in mycelium coherence:

Drought onset. Soil moisture reduction causes mycelium spiking frequency to decrease and inter-spike interval variability to increase, producing a measurable decline in $P(t)$ (pattern

retention) and $A(t)$ (phase alignment across electrodes). Based on published mycelium electrophysiology data [Adamatzky, 2018a], we expect detectable coherence changes (Δ decline >15% from baseline) within 6–24 hours of soil moisture dropping below the species-specific stress threshold.

Chemical contamination. Heavy metals and organic pollutants alter mycelium metabolic activity and growth patterns, producing changes in spiking amplitude, frequency, and impedance. The coherence engine detects these as anomalous drift (D increase) and pattern disruption (P decrease) without needing to know the specific contaminant.

Seasonal transitions. Multi-scale coherence analysis (1-hour, 24-hour, 7-day windows) captures diurnal activity cycles, weather-related fluctuations, and seasonal dormancy transitions. The 24-hour window Δ provides the most stable baseline for detecting non-seasonal anomalies.

7 Additional Application Domains

While we have developed structural health monitoring and ecological monitoring in detail, the six-layer architecture applies to additional domains that we outline briefly. Table 1 summarizes configurations across all five application areas.

Domain	Scaffold	Sensing	Energy	Processing	Mode
Structural health	Mycelium in concrete	Strain, impedance, electrical, acoustic	Grid + MFC	Edge compute	Adaptive
Ecological monitoring	Mycelium in soil	Electrical, moisture, pH, temp	Solar + MFC	Edge (RPi)	Observation
Materials science	Biofilm on substrate	Impedance, chemical, optical	Lab power	Desktop	Perturbation
Deep-sea sensing	Biomineralized + biofilm	Pressure, chemical, temp	MFC + thermal	Low-power MCU	Autonomous
Space / off-world	Hybrid scaffold	Electrical, temp	MFC + solar	Rad-hard MCU	Autonomous

Table 1: Application domain configurations. Bold rows indicate the two applications developed in detail in this paper. Each domain selects scaffold type, sensing modalities, energy strategy, processing hardware, and default operational mode based on environmental constraints.

Materials science. Biofilm scaffolds grown on engineered substrates provide living platforms for studying material-biology interfaces under controlled perturbation (antibiotic exposure, nutrient deprivation, temperature cycling). The coherence engine enables adaptive experimental protocols that respond to biofilm state rather than following fixed schedules.

Deep-sea sensing. At depths where battery replacement is prohibitively expensive and solar power is unavailable, chemosynthetic microbial communities at hydrothermal vents or cold seeps could generate power from chemical gradients while providing sensing capabilities. This application requires advances in pressure-tolerant biological scaffolds and remains at the conceptual stage.

Off-world infrastructure. Mycelium-based biocomposites grown from local regolith and minimal organic feedstock have been demonstrated at laboratory scale by NASA's Myco-Architecture project [Rothschild, 2019], and ESA's MELiSSA project provides closed-loop

life support technology using microbial bioreactors [Lasseur et al., 2010]. Integrating coherence monitoring into these biological construction systems could detect degradation from radiation exposure or nutrient depletion. This application requires substantial further development in radiation-tolerant scaffold biology and closed-loop nutrient cycling, and we note it as a long-term research direction rather than a near-term engineering target.

8 Connection to the Coherence Framework

The coherence operator $\Delta = (P \cdot A \cdot R)/(D + N)$ was derived from dynamical systems theory, recurrence quantification analysis, and information geometry [Thorarinson and Hensgen, 2026]. These mathematical tools apply to any system producing a multivariate time series with recurrence structure — which includes every living biological system measured with sufficient temporal resolution.

Proposition 1 (Biological Coherence Measurability)**.** *Any biological scaffold $\mathcal{B}$ with measurable electrical, chemical, or mechanical dynamics produces a time series $\mathbf{x}(t)$ with nonzero recurrence rate $RR > 0$ and positive determinism $DET > 0$ during healthy operation. Therefore the coherence operator $\Delta(\mathbf{x}(t))$ is well-defined and produces values in the range $(0, \infty)$.*

This follows from the observation that living systems maintain homeostasis, exhibit periodic processes (metabolic cycles, circadian rhythms, growth oscillations), and respond to perturbations by returning toward equilibrium states. These properties produce exactly the recurrence structure that the coherence operator measures.

The connection also runs in the reverse direction. The seven validation domains in Thorarinson and Hensgen [2026] — engines, valves, power grids, hearts, brains, financial systems, and synthetic benchmarks — form a spectrum from purely mechanical to purely biological. Bio-integrated infrastructure occupies a natural position on this spectrum: systems where biological and engineered components operate together, and coherence measures the health of the coupled system.

The biological dimension adds a feature absent from purely engineered systems: the scaffold's coherence is not merely an indicator of system state but a product of the distributed bioelectric intelligence that Levin has characterized across biological scales [Levin, 2021, 2023, McMillen and Levin, 2024]. When the coherence engine detects declining Δ_{bio}, it is detecting a loss of the collective coordination that keeps the biological scaffold functional — the same coordination mechanism that drives embryogenesis, regeneration, and wound healing in other biological contexts.

9 Prototype Design and Cost Estimate

A working prototype for the ecological monitoring application (Application 2) is buildable with off-the-shelf components. Table 2 provides the bill of materials.

9.1 Timeline

1. **Scaffold preparation** (weeks 1–3): Inoculate wood-chip substrate with *P. ostreatus* spawn. Full colonization in 2–4 weeks at 20–25°C and 80–90% humidity. Assemble electronics: wire electrode pairs to ADS1299 breakout, connect environmental sensors to Raspberry Pi GPIO/I2C.

2. **Software setup** (week 2, concurrent): Install signal processing pipeline (Python, NumPy, SciPy). Implement coherence engine (Δ operator computation). Set up dashboard (Flask + Plotly or Grafana). Total software: approximately 800–1200 lines of Python, with the coherence engine core reused from Thorarinson and Hensgen [2026].

Component	Specification	Est. Cost (USD)
Raspberry Pi 4	4 GB RAM, 32 GB SD card	\$55–75
ADS1299 breakout board	8-channel, 24-bit ADC	\$30–50
Stainless steel electrodes	1 mm dia., 8 pcs	\$5–10
SHT31 sensor	Temperature / humidity	\$5–8
Capacitive soil moisture sensor	Analog output	\$3–5
5 W solar panel	12 V output	\$15–25
LiPo battery + charge controller	10 Wh, 3.7 V	\$15–25
Pleurotus ostreatus spawn	Grain spawn, 1 kg	\$10–15
Wood-chip substrate + container	Hardwood chips, 30×30×10 cm	\$5–10
Enclosure & wiring	Weatherproof box, connectors, cables	\$20–40
MFC components (optional)	Carbon felt electrodes, membrane	\$15–30
Total (without MFC)		**\$163–263**
Total (with MFC)		**\$178–293**

Table 2: Bill of materials for the ecological monitoring prototype. Prices reflect 2026 retail pricing for single-unit quantities; bulk deployment would reduce per-unit cost by 30–50%.

3. **Deployment and baseline** (days 1–3 after colonization): Insert electrodes into colonized substrate. Deploy at monitoring site. Run observation mode. Establish baseline Δ_{bio} distribution.

4. **Perturbation mapping** (days 4–10): Controlled perturbations — moisture reduction (let substrate dry 10%), temperature step (±5°C for 1 hour), mechanical tap (standardized impact). Measure coherence response and recovery time for each perturbation type.

5. **Stress test** (days 11–14): Sustained environmental stress (reduced moisture, elevated temperature). Track coherence trajectory. Verify that Δ declines before visible signs of mycelium distress.

6. **Recovery** (days 15–17): Restore optimal conditions. Verify coherence recovery. Validate Windowed Recovery operator $W(t)$ predictions.

Total timeline from project start to validated prototype: 5–6 weeks. Total materials cost: \$180–\$350 including optional MFC and contingency.

10 Discussion

10.1 What Bio-Integration Adds

Bio-integrated infrastructure does not replace conventional infrastructure. A bridge still needs steel. A building still needs concrete. The proposal is to add a biological layer that provides capabilities conventional materials cannot: self-repair, distributed environmental sensing at high spatial density, adaptive structural response, and continuous health reporting through living dynamics. The coherence engine converts the biological system's inherent distributed intelligence — the bioelectric coordination mechanisms described by Levin [2021] — into actionable infrastructure data.

10.2 Limitations

Biological systems introduce constraints that engineered systems do not have:

Variability. No two mycelium networks grow identically. Baseline coherence levels, response characteristics, and recovery dynamics differ between instances. The coherence engine handles

this through per-instance baseline establishment rather than universal thresholds, as detailed in Section 3.5.1.

Timescales. Biological processes operate on timescales from seconds (spiking) to months (growth, colonization). The signal processing layer must handle this range, and the coherence engine must distinguish slow biological drift (normal growth) from pathological drift (degradation). Multi-scale Δ computation at multiple window sizes addresses this but adds computational cost.

Environmental coupling. Biological scaffolds are sensitive to temperature, humidity, pH, and nutrient availability. A change in coherence may reflect environmental change rather than scaffold degradation. The conditional threshold approach (Section 3.5.1) mitigates this but requires adequate environmental sensor coverage and sufficient baseline data across the expected environmental range.

Sterility and contamination. In controlled environments, maintaining the intended biological community requires contamination control. In open environments (soil, concrete surfaces), the scaffold interacts with ambient microbial communities, potentially altering its dynamics. The coherence engine detects these interactions as changes in recurrence structure but cannot distinguish beneficial colonization from harmful contamination without biological domain knowledge.

Longevity. Engineered sensors last years to decades. Biological scaffolds have natural lifespans and may require renewal. The architecture accommodates this through modular scaffold replacement and the coherence engine's ability to re-establish baselines.

Unvalidated biological thresholds. The coherence thresholds in this paper are transferred from engineering domains. While the mathematical framework is substrate-agnostic, the specific threshold values ($\Delta = 0.7, 0.3$) have not been validated on biological time series. The prototype experimental protocol (Section 7.1) is designed to produce this validation data, but until it is collected, the biological thresholds should be treated as provisional.

10.3 Advantages

Despite these limitations, biological scaffolds provide properties unavailable in manufactured materials:

Self-repair. Mycelium networks regrow through damaged regions. Bio-concrete heals cracks up to 0.8 mm through metabolically driven calcite precipitation [Jonkers et al., 2010]. Living building materials can regenerate entirely [Heveran et al., 2020]. No manufactured sensor network repairs itself.

Distributed sensing at high spatial density. A mycelium network covers square meters to hectares with each hyphal tip acting as a transducer. Manufacturing an equivalent sensor network at this density is economically impractical.

Low embodied energy. Biological scaffolds grow from low-energy feedstocks (agricultural waste, ambient nutrients). The embodied energy of a mycelium scaffold is orders of magnitude lower than an equivalent mass of manufactured sensor hardware.

Carbon sequestration. Mycelium and biomineralized scaffolds sequester atmospheric carbon during growth, making bio-integrated infrastructure potentially carbon-negative.

10.4 Future Directions

Three research directions would advance bio-integrated infrastructure from prototype to deployment:

Biological threshold validation. Systematic measurement of coherence operator values on biological time series across scaffold types, environmental conditions, and degradation modes. This requires collecting the dataset described in the prototype protocol (Section 7.1) and repeating it across species, substrates, and stress types to build a biological calibration library analogous to the engineering datasets used in Thorarinson and Hensgen [2026].

Multi-node spatial coherence. Extending the single-node coherence computation to spatial coherence maps across networks of bio-integrated nodes. Cross-correlation of Δ across spatially distributed nodes could detect propagating environmental transitions (drought fronts, contamination plumes) with directional and velocity information.

Extreme environment applications. The deep-sea and off-world applications outlined in Section 6 require advances in pressure-tolerant and radiation-tolerant scaffold biology that are beyond current technology readiness. We note these as motivating targets for the architecture rather than near-term engineering objectives.

11 Conclusion

The six-layer architecture presented here connects living biological dynamics to engineering decision-making through a defined stack: biological scaffolds provide the substrate, sensors make biological dynamics observable, signal processing extracts state variables, and the coherence engine — validated across seven engineered domains [Thorarinson and Hensgen, 2026] — assesses system health through the same operator $\Delta = (P \cdot A \cdot R)/(D + N)$ that detects turbofan degradation 185 cycles before failure. The operator works on biological systems because both engineered and living systems exhibit the same mathematical signatures when losing structural coherence: declining pattern retention, desynchronization, and reduced recovery capacity.

We have developed two applications in detail. In structural health monitoring, the architecture combines conventional strain sensing with biological channels (mycelium spiking, bacterial impedance) to monitor both structural integrity and self-healing capacity — a capability absent from current SHM systems. In ecological monitoring, soil-embedded mycelium networks provide distributed biological sensing at spatial densities impractical with manufactured sensors, with the coherence engine detecting environmental transitions as changes in the mycelium's bioelectric coordination.

The near-term path is a hybrid prototype buildable in 5–6 weeks for $180–$350: a mycelium substrate monitored by conventional sensors, processed by a Raspberry Pi, and assessed by a Python implementation of the coherence engine. This prototype will produce the biological time series data needed to validate coherence thresholds for living systems and to test whether the substrate-agnostic mathematical framework transfers from engineering to biology as the theory predicts.

References

Andrew Adamatzky. On spiking behaviour of oyster fungi *Pleurotus djamor*. *Scientific Reports*, 8(1):7873, 2018a.

Andrew Adamatzky. Towards fungal computer. *Interface Focus*, 8(6):20180029, 2018b. doi: 10.1098/rsfs.2018.0029.

Ryan P Adams and David JC MacKay. Bayesian online changepoint detection. *arXiv preprint arXiv:0710.3742*, 2007. URL https://arxiv.org/abs/0710.3742.

Rachel Armstrong. *Living Architecture: How Synthetic Biology Can Remake Our Cities and Reshape Our Lives*. TED Books, 2012.

Elise Elsacker, Simon Vandelook, Joost Brancart, Eveline Peeters, and Lars De Laet. Mechanical, physical and chemical characterisation of mycelium-based composites with different types of lignocellulosic substrates. *PLoS ONE*, 14(7):e0213954, 2019. doi: 10.1371/journal.pone.0213954.

Charles R Farrar and Keith Worden. An introduction to structural health monitoring. *Philosophical Transactions of the Royal Society A*, 365(1851):303–315, 2007. doi: 10.1098/rsta.2006.1928.

Muhammad Haneef, Luca Ceseracciu, Claudio Canale, Ilker S Bayer, Jose A Heredia-Guerrero, and Athanassia Athanassiou. Advanced materials from fungal mycelium: Fabrication and tuning of physical properties. *Scientific Reports*, 7:41292, 2017.

Chelsea M Heveran, Sarah L Williams, Jishen Qiu, Juliana Artier, Mija H Hubler, Sherri M Cook, Jeffrey C Cameron, and Wil V Srubar. Biomineralization and successive regeneration of engineered living building materials. *Matter*, 2(2):481–494, 2020. doi: 10.1016/j.matt.2019.11.016.

Henk M Jonkers, Arjan Thijssen, Gerard Muyzer, Oguzhan Copuroglu, and Erik Schlangen. Application of bacteria as self-healing agent for the development of sustainable concrete. *Ecological Engineering*, 36(2):230–235, 2010. doi: 10.1016/j.ecoleng.2008.12.036.

Sourabh Kumar, Kristine Boone, Jack Tuszyński, Paul Barclay, and Christoph Simon. Possible existence of optical communication channels in the brain. *Scientific Reports*, 6:36508, 2016. doi: 10.1038/srep36508.

Christophe Lasseur, Jean Brunet, Hatim de Weever, Mike Dixon, Claude-Gilles Dussap, and Francesc Godia. MELiSSA: The European project of closed life support system. *Gravitational and Space Biology*, 23(2), 2010.

Michael Levin. Bioelectric signaling: Reprogrammable circuits underlying embryogenesis, regeneration, and cancer. *Cell*, 184(6):1971–1989, 2021.

Michael Levin. Bioelectric networks: The cognitive glue enabling evolutionary scaling. *Animal Cognition*, 26:1865–1891, 2023.

Bruce E Logan. *Microbial Fuel Cells*. John Wiley & Sons, Hoboken, NJ, 2008.

Bruce E Logan. Exoelectrogenic bacteria that power microbial fuel cells. *Nature Reviews Microbiology*, 7(5):375–381, 2009. doi: 10.1038/nrmicro2113.

Bruce E Logan, Bert Hamelers, René Rozendal, Uwe Schröder, Jürg Keller, Stefano Freguia, Peter Aelterman, Willy Verstraete, and Korneel Rabaey. Microbial fuel cells: Methodology and technology. *Environmental Science & Technology*, 40(17):5181–5192, 2006.

Patrick McMillen and Michael Levin. Collective intelligence: A unifying concept for integrating biology across scales. *Communications Biology*, 7:378, 2024.

William J Mitsch and Sven Erik Jørgensen. *Ecological Engineering and Ecosystem Restoration*. John Wiley & Sons, New York, 2004.

Peter Q Nguyen, Zsofia Botyanszki, Pei Kun R Tay, and Neel S Joshi. Programmable biofilm-based materials from engineered curli nanofibres. *Nature Communications*, 5:4945, 2014. doi: 10.1038/ncomms5945.

Hamza Patwa, Nathan S. Babcock, and Philip Kurian. Quantum-enhanced photoprotection in neuroprotein architectures emerges from collective light-matter interactions. *Frontiers in Physics*, 12:1387271, 2024. doi: 10.3389/fphy.2024.1387271.

Lynn J Rothschild. Myco-architecture off planet: Growing surface structures at destination. NIAC phase I final report, NASA Ames Research Center, 2019. URL https://ntrs.nasa.gov/citations/20190002580.

Tzu-Chieh Tang, Bolin An, Yuanyuan Huang, Sangram Vasikaran, Yanyi Wang, Xiaoyu Jiang, Timothy K Lu, and Chao Zhong. Materials design by synthetic biology. *Nature Reviews Materials*, 6(4):332–350, 2021. doi: 10.1038/s41578-020-00265-w.

Joel Thorarinson and Allison Hensgen. From prediction to discoverative intelligence: A coherence-based AI framework for detecting system drift before failure. *arXiv preprint*, 2026.

Jan Roelof van der Meer and Shimshon Belkin. Where microbiology meets microengineering: Design and applications of reporter bacteria. *Nature Reviews Microbiology*, 8(7):511–522, 2010. doi: 10.1038/nrmicro2392.

Andrea Zangari, Davide Micheli, Roberta Galeazzi, and Antonio Tozzi. Node of Ranvier as an array of bio-nanoantennas for infrared communication in nerve tissue. *Scientific Reports*, 8: 539, 2018. doi: 10.1038/s41598-017-18866-x.